Joint 3D inversion of marine CSEM and MT data

Alexander V. Gribenko and Michael S. Zhdanov, University of Utah and TechnoImaging*

Summary

Magnetotelluric (MT) data naturally manifests itself as noise in marine controlled-source electromagnetic (CSEM) data. It follows that MT data can be extracted from measured CSEM data for the relatively negligible cost of additional data processing. With availability of both data sets, we present a new approach to 3D joint inversion of both CSEM and MT data. Our method is based on the 3D integral equation method for modeling, and focusing regularized inversion. Our examples show that joint CSEM and MT inversion has better model resolution compared to CSEM or MT inversion alone.

Introduction

The premise of various marine controlled-source electromagnetic (CSEM) methods is that their responses are sensitive to the lateral extents and thicknesses of resistive bodies embedded in conductive hosts. Hence, the initial applications have been for de-risking exploration and appraisal projects with direct hydrocarbon indication (Hesthammer et al., 2010). CSEM methods are based on the transmission of low-frequency electromagnetic (EM) signals from a towed source and measurement of the EM responses using an array of seafloor receivers. CSEM receivers often have broad bandwidths, so they also measure magnetotelluric (MT) signals, which are considered as noise in CSEM data. It follows that MT data can be extracted from CSEM time-series data for the relatively negligible cost of additional data processing. Inclusion of MT data can provide additional constraints on CSEM data, and reduce uncertainty on subsequent interpretations. There are several commercial solutions available for 3D inversion of either CSEM or MT data, but few solutions are available for joint CSEM and MT inversion (e.g., Mackie et al., 2007; Abubakar et al., 2009; Commer and Newman, 2009). In this paper, we present our methodology for 3D joint inversion of CSEM and MT data. This is an extension of our previous work on both 3D CSEM inversion (e.g., Zhdanov et al., 2010) and 3D MT inversion (e.g., Zhdanov et al., 2011a).

3D modeling

The 3D CSEM modeling problem can be written in operator form as

$$\mathbf{d}^{CSEM} = A^{CSEM}(\boldsymbol{\sigma}), \tag{1}$$

where $\mathbf{d}^{CSEM}$ is the N_d length vector of observed CSEM data, $\boldsymbol{\sigma}$ is the N_m length vector of the 3D conductivity distribution in the 3D model, and A^{CSEM} is a nonlinear operator based on a discrete form of Maxwell's equations. Similarly, the 3D MT modeling problem can be written in operator form as:

$$\mathbf{d}^{MT} = A^{MT}(\boldsymbol{\sigma}), \tag{2}$$

where $\mathbf{d}^{MT}$ is the N_d length vector of observed MT data, $\boldsymbol{\sigma}$ is the N_d length vector of the 3D conductivity distribution in the 3D model, and A^{CSEM} is a nonlinear operator based on a discrete form of Maxwell's equations and inclusive of the MT transfer functions. The nonlinear operators in equations (1) and (2) may be representative of finite-difference, finite-element, or integral equation methods (Zhdanov, 2009). The advantage of integral equation methods is that the entire 3D earth model need not be discretized. Rather, an appropriate background conductivity model is chosen, and only those volumes of interest containing deviations from the background conductivity need to be discretized. This is unlike finite-difference or finite-element methods, which require whole-space discretization and an appropriate choice of boundary conditions so as to emulate an unbound 3D earth model.

Following the separation of the 3D earth model into background (*b*) and anomalous (*a*) conductivity models, we can derive a vector Fredholm integral equation of the second kind for the anomalous electric fields inside the volumes of interest:

$$\mathbf{E}^a(\mathbf{r}') = \int_V \hat{\mathbf{G}}_E(\mathbf{r}', \mathbf{r}) \cdot \sigma_a(\mathbf{r})[\mathbf{E}^b(\mathbf{r}) + \mathbf{E}^b(\mathbf{r})]dv, \tag{3}$$

where $\hat{\mathbf{G}}_E(\mathbf{r}', \mathbf{r})$ are the electric Green's tensors for the background conductivity model. Using the method of moments, equation (3) can be reduced to the linear system:

$$\mathbf{E}^a = (\mathbf{I} - \boldsymbol{\Gamma}\boldsymbol{\sigma}_a)^{-1} \cdot \boldsymbol{\Gamma} \cdot \boldsymbol{\sigma}_a \cdot \mathbf{E}^b, \tag{4}$$

where $\mathbf{E}^a$ is the vector of the anomalous electric field, $\mathbf{I}$ is the identity matrix, $\boldsymbol{\Gamma}$ is the matrix of volume-integrated electric Green's tensors for the background conductivity model, and $\boldsymbol{\sigma}_a$ is a diagonal matrix of anomalous conductivities. The electric and magnetic fields at the receivers can then be calculated from the following equations:

$$\mathbf{E}(\mathbf{r}') = \mathbf{E}^b(\mathbf{r}') + \int_V \hat{\mathbf{G}}_E(\mathbf{r}', \mathbf{r}) \cdot \sigma_a(\mathbf{r})[\mathbf{E}^b(\mathbf{r}) + \mathbf{E}^b(\mathbf{r})]dv,$$
$$\mathbf{H}(\mathbf{r}') = \mathbf{H}^b(\mathbf{r}') + \int_V \hat{\mathbf{G}}_H(\mathbf{r}', \mathbf{r}) \cdot \sigma_a(\mathbf{r})[\mathbf{E}^b(\mathbf{r}) + \mathbf{E}^b(\mathbf{r})]dv. \tag{5}$$

© 2011 SEG

Joint 3D inversion of marine CSEM and MT data

Equation (5) requires the total electric field in each cell, and this is computed as the sum of the background and anomalous electric fields. For models with high conductivity contrasts or very resistive hosts, the background and anomalous electric fields are of near-equal amplitude but opposite sign. Given finite precision, their addition introduces numerical errors. By adding the background electric fields to both sides of equation (4), we obtain the linear system:

$$\mathbf{E} = (\mathbf{I} - \mathbf{\Gamma}\boldsymbol{\sigma}_a)^{-1} \cdot \mathbf{E}^b, \qquad (6)$$

which solves for the total electric field, $\mathbf{E}$, instead of the anomalous electric field while retaining the distributed source in terms of the background electric fields. This improves accuracy, and is a unique feature of the integral equation method. However, evaluating $\mathbf{E}$ requires the solution of a large, dense, and ill-conditioned matrix system. Following Hursán and Zhdanov (2002), we precondition equation (6) with contraction operators to improve the conditioning of the matrix system. We also exploit the Toeplitz structure of matrix system (6), meaning that we can perform multiplications of the translationally invariant horizontal components of $\mathbf{\Gamma}$ without needing to store its full size. We solve system (6) using the complex generalized minimum-residual method (CGMRES), as this has been proven to always converge (Zhdanov, 2002). With equidistant discretization of the 3D model in each of the *x* and *y* directions, matrix-vector multiplications in the CGMRES solution to matrix equation (6) can be provided by 2D FFT convolutions that further reduce computational complexity from $O(n^2)$ to $O(n\log n)$.

Inversion methodology

To solve both CSEM and MT inverse problems, we use a variant of Tikhonov regularization, viz.:

$$P(\boldsymbol{\sigma}_a) = W_d^{CSEM}\varphi^{CSEM}(\boldsymbol{\sigma}_a) + W_d^{MT}\varphi^{MT}(\boldsymbol{\sigma}_a) + S(\boldsymbol{\sigma}_a), \qquad (7)$$

where W_d^{CSEM} and W_d^{MT} are CSEM and MT data weights, φ^{CSEM} and φ^{MT} are CSEM and MT misfit functionals, and $S(\boldsymbol{\sigma}_a)$ is a stabilizing functional. Given the different dynamic ranges of CSEM and MT data, we need to introduce the data weights to balance the CSEM and MT data during inversion. We choose both data weights in a similar fashion, i.e.:

$$W_d = \sqrt{\mathrm{mean}(\varphi_0)}, \qquad (8)$$

where φ_0 is the misfit for the initial model. We have included a variety of stabilizing functionals, including both smooth and focusing options (e.g., Zhdanov et al., 2010).

To minimize equation (7), we use the regularized re-weighted conjugate gradient (RRCG) method (Zhdanov, 2002). To solve for the regularized direction of steepest descent, we calculate the Fréchet derivatives of the electric and/or magnetic fields using the quasi-Born approximation (Gribenko and Zhdanov, 2007):

$$\mathbf{F}_{E,H}(\mathbf{r}') = \widehat{\mathbf{G}}_{E,H}(\mathbf{r}', \mathbf{r})\mathbf{E}(\mathbf{r}). \qquad (9)$$

Sensitivities for CSEM data or MT transfer functions can be derived from solutions to equation (9). All CSEM components can be considered, as well as any combinations of the MT impedance tensor and/or tipper components.

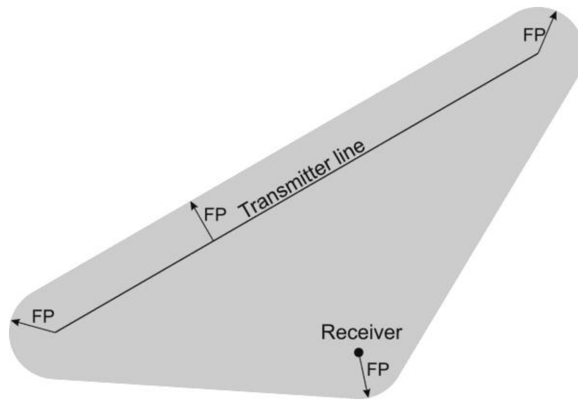

Figure 1. *CSEM footprint is shown by gray area, where FP stands for footprint distance.*

To further reduce computational speed and computer memory requirements, we applied a footprint approach. Cox et al. (2010) introduced this approach for airborne EM (AEM) inversion, and Zhdanov et al. (2011b) applied it for large-scale MT inversion. Unlike AEM or MT inversion, footprint in CSEM inversion has to cover a large volume including both the transmitter line(s) and receiver positions. CSEM sensitivities are computed and stored only within the footprint distance of a receiver and the corresponding transmitter line. The area between the transmitter line and the receiver is also included in the CSEM footprint (Figure 1). MT sensitivities are computed and stored only for regions that are much smaller than the whole inversion domain, i.e., within a footprint distance from the station. This footprint approach provides a dramatic reduction in required computer memory. We note that, unlike Cox et al. (2010), we only use the footprint for the sensitivity computation and storage. Modeling is based on the entire 3D model to ensures accuracy in the predicted fields, as well as the domain electric fields used in equation (9).

© 2011 SEG

Joint 3D inversion of marine CSEM and MT data

Model study

To demonstrate our joint CSEM and MT inversion, we have considered a combination of targets, namely a large salt dome and a thin hydrocarbon-bearing reservoir adjacent to it. The former target is more suitable for MT inversion, while the latter would be best suited to CSEM inversion. A vertical cross section and a 3D view of this model are shown in Figures 2 and 3, respectively. The receiver locations are shown by circles in Figure 3. They form a grid of 12 profiles with 20 receivers along each line, each separated by 500 m. Synthetic principal component MT impedances were computed at 240 receiver locations at seven frequencies: 0.001 Hz, 0.003 Hz, 0.01 Hz, 0.03 Hz, 0.1 Hz, 0.3 Hz, and 1 Hz. CSEM data were computed for the same receivers at the fundamental frequency of 0.125 Hz. One transmitter line was used, with both inline and azimuthal electric fields measured across the receiver array.

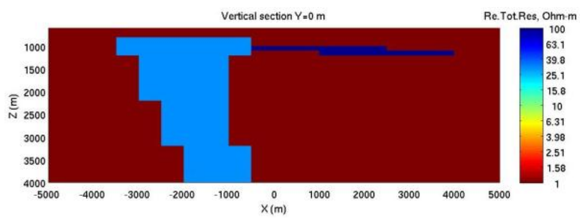

Figure 2. *Vertical cross section through the 3D earth model of a salt dome and adjacent hydrocarbon-bearing reservoir.*

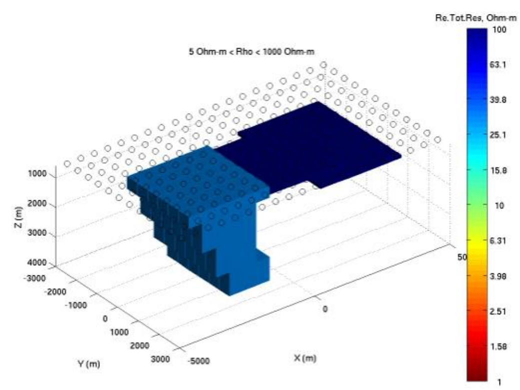

Figure 3. *3D perspective of the salt dome and adjacent hydrocarbon-bearing reservoir. Receiver positions are shown by circles.*

We first inverted both MT and MCSEM data separately. Figures 4 and 5 show vertical cross sections through the MT and CSEM inversion results, respectively. The MT inversion recovered the salt dome with better accuracy than the CSEM inversion. At the same time, MT inversion was not sensitive to the hydrocarbon-bearing reservoir. On the other hand, CSEM inversion recovered the horizontal locations of both the reservoir and the salt dome, but did not recover the depth extent of the salt dome. These results are not unexpected.

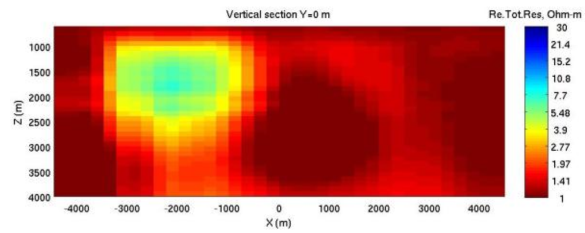

Figure 4. *Vertical cross section through the 3D earth model recovered from 3D MT inversion.*

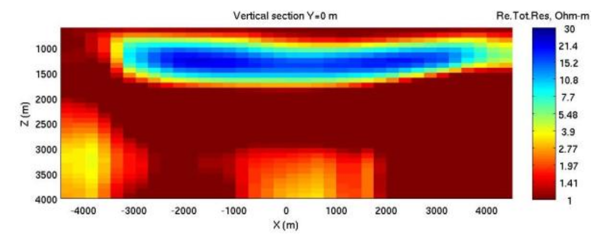

Figure 5. *Vertical cross section through the 3D earth model recovered from 3D CSEM inversion.*

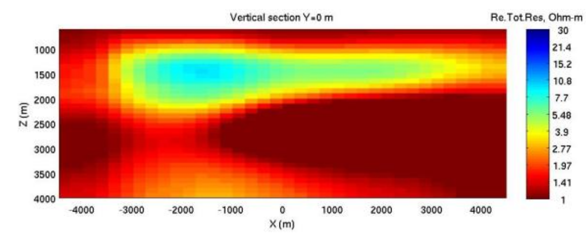

Figure 6. *Vertical cross section through the 3D earth model recovered from 3D joint MT and CSEM inversion.*

Figure 6 shows the vertical section through the joint CSEM and MT inversion result. Both the salt dome and the hydrocarbon-bearing reservoir were recovered. Figures 7 and 8 show observed and predicted TM and TE apparent resistivity and phase maps for an intermediate frequency of 0.01 Hz. Figures 9 and 10 show observed and predicted curves of the CSEM fields for an inline and an azimuthal receiver. We note both MT and CSEM data are fitted well.

© 2011 SEG

Joint 3D inversion of marine CSEM and MT data

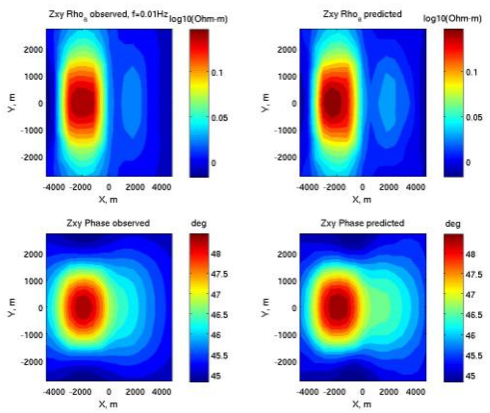

Figure 7. *Observed (left panels) and predicted (right panels) Zxy apparent resistivity (upper panels) and phase (lower panels) for 0.1 Hz.*

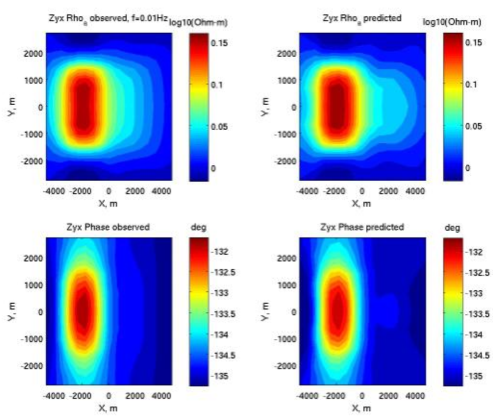

Figure 8. *Observed (left panels) and predicted (right panels) Zyx apparent resistivity (upper panels) and phase (lower panels) for 0.1 Hz.*

Conclusions

We have developed a methodology for 3D joint inversion of CSEM and MT data, capable of inverting any combination of receivers, transfer functions and frequencies. We have introduced a receiver footprint approach and quasi-Born approximation for efficient Fréchet derivative calculation. We have tested this method on a synthetic model of a salt dome and hydrocarbon-bearing reservoir. The results of these tests demonstrate that joint CSEM and MT inversion recovers improved subsurface images over inversion by either method alone.

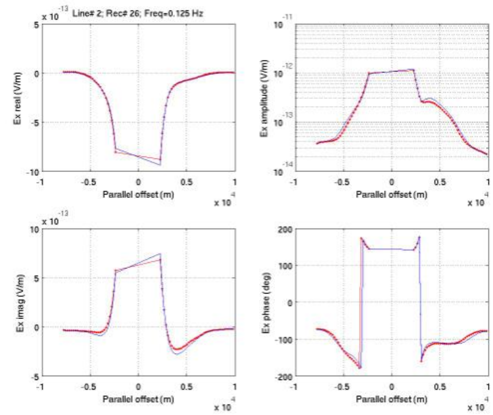

Figure 9. *Example of observed (blue) and predicted (red) data for inline electric field receiver for 0.125 Hz.*

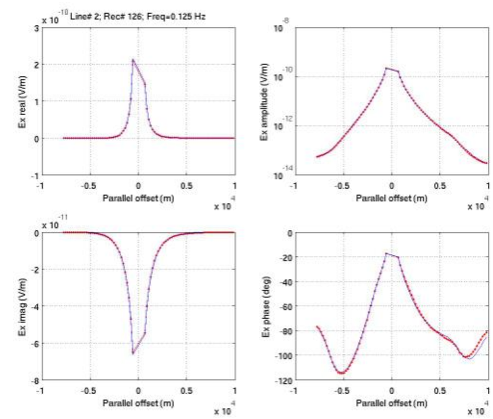

Figure 9. *Example of observed (blue) and predicted (red) data for azimuthal electric field receiver for 0.125 Hz.*

Acknowledgements

The authors acknowledge support of the University of Utah's Consortium for Electromagnetic Modeling and Inversion (CEMI), and TechnoImaging for permission to publish.

© 2011 SEG

EDITED REFERENCES

Note: This reference list is a copy-edited version of the reference list submitted by the author. Reference lists for the 2011 SEG Technical Program Expanded Abstracts have been copy edited so that references provided with the online metadata for each paper will achieve a high degree of linking to cited sources that appear on the Web.

REFERENCES

Abubakar, A., M. Li, J. Liu, and T. M. Habashy, 2009, Simultaneous joint inversion of MT and CSEM data using a multiplicative cost function: 79th Annual International Meeting, SEG, Expanded Abstracts, 719–723, doi:10.1190/1.3255855.

Commer, M., and G. A. Newman, 2009, Three-dimensional controlled-source electromagnetic and magnetotelluric joint inversion: Geophysical Journal International, **178**, 1305–1316, doi:10.1111/j.1365-246X.2009.04216.x.

Cox, L. H., G. A. Wilson, and M. S. Zhdanov, 2010, 3D inversion of airborne electromagnetic data using a moving footprint: Exploration Geophysics, **41**, 250–259, doi:10.1071/EG10003.

Gribenko, A., and M. S. Zhdanov, 2007, Rigorous 3D inversion of marine CSEM data based on the integral equation method: Geophysics, **72**, no. 2, WA73–WA84, doi:10.1190/1.2435712.

Hesthammer, J., A. Stefatos, M. Boulaenko, S. Fanavoll, and J. Danielsen, 2010, CSEM performance in light of well results: The Leading Edge, **29**, 34–41, doi:10.1190/1.3284051.

Hursán, G., and M. S. Zhdanov, 2002, Contraction integral equation method in three-dimensional electromagnetic modeling: Radio Science, **37**, 1089–1101, doi:10.1029/2001RS002513.

Mackie, R., M. D. Watts, and W. Rodi, 2007, Joint 3D inversion of marine CSEM and MT data: 77th Annual International Meeting, SEG, Expanded Abstracts, 574–578, doi:10.1190/1.2792486.

Zhdanov, M. S., 2002, Geophysical inverse theory and regularization problems: Elsevier.

Zhdanov, M. S., 2009, Geophysical electromagnetic theory and methods: Elsevier.

Zhdanov, M. S., R. B. Smith, A. Gribenko, M. Čuma, and A. M. Green, 2011b, Three-dimensional inversion of large-scale EarthScope magnetotelluric data based on the integral equation method: Geoelectrical imaging of the Yellowstone conductive mantle plume: Geophysical Research Letters, **38,** L08307–L08313, doi:10.1029/2011GL046953.

Zhdanov, M. S., E. P. Velikhov, M. Čuma, G. Wilson, N. Black, and A. Gribenko, 2010, Exploring multiple 3D inversion scenarios for enhanced interpretation of marine CSEM data: an iterative migration analysis of the Shtokman gas field: First Break, **28**, 95–101.

Zhdanov, M. S., L. Wan, A. Gribenko, M. Čuma, K. Key, and S. Constable, 2011a, Large-scale 3D inversion of marine magnetotelluric data: Case study from the Gemini prospect, Gulf of Mexico: Geophysics, **76**, no. 1, F77–F87, doi:10.1190/1.3526299.

© 2011 SEG